Light-controlled twister ribozyme with single-molecule detection resolves RNA function in time and space

Arthur Korman[a,1,2], Huabing Sun[b,1,3], Boyang Hua[c], Haozhe Yang[b], Joseph N. Capilato[b], Rakesh Paul[b,4], Subrata Panja[d,5], Taekjip Ha[c,e,f], Marc M. Greenberg[b,6], and Sarah A. Woodson[d,6]

[a]Cell, Molecular, Developmental Biology and Biophysics Program, Johns Hopkins University, Baltimore, MD 21218; [b]Department of Chemistry, Johns Hopkins University, Baltimore, MD 21218; [c]Department of Biophysics and Biochemistry, Johns Hopkins University, Baltimore, MD 21205-2185; [d]T. C. Jenkins Department of Biophysics, Johns Hopkins University, Baltimore, MD 21218; [e]Department of Biomedical Engineering, Johns Hopkins University, Baltimore, MD 21218; and [f]Howard Hughes Medical Institute, Johns Hopkins University, Baltimore, MD 21205

Edited by Michael F. Summers, University of Maryland, Baltimore County, Baltimore, MD, and approved April 3, 2020 (received for review February 22, 2020)

Small ribozymes such as *Oryza sativa* twister spontaneously cleave their own RNA when the ribozyme folds into its active conformation. The coupling between twister folding and self-cleavage has been difficult to study, however, because the active ribozyme rapidly converts to product. Here, we describe the synthesis of a photocaged nucleotide that releases guanosine within microseconds upon photosolvolysis with blue light. Application of this tool to *O. sativa* twister achieved the spatial (75 μm) and temporal (≤30 ms) control required to resolve folding and self-cleavage events when combined with single-molecule fluorescence detection of the ribozyme folding pathway. Real-time observation of single ribozymes after photo-deprotection showed that the precleaved folded state is unstable and quickly unfolds if the RNA does not react. Kinetic analysis showed that Mg^{2+} and Mn^{2+} ions increase ribozyme efficiency by making transitions to the high energy active conformation more probable, rather than by stabilizing the folded ground state or the cleaved product. This tool for light-controlled single RNA folding should offer precise and rapid control of other nucleic acid systems.

photocaged nucleotide | single-molecule FRET | RNA folding | nucleic acid chemistry | ribozyme catalysis

Small self-cleaving ribozymes are found in diverse species and have been widely studied for their applications to gene regulation and sensing, therapeutics, and the origins of life (1). Because self-cleavage occurs spontaneously once the ribozyme folds into an active conformation, ribozyme performance is linked to the RNA folding dynamics. For example, single-molecule Förster resonance energy transfer (smFRET) studies showed that fluctuations between folded and unfolded hairpin ribozymes regulate the internal equilibrium between self-cleavage and ligation (2, 3). Long-range tertiary interactions that stabilize the global structure of the various ribozymes also favor reorganization of their active sites, leading to higher rates of catalysis (4–9). It has been nevertheless challenging to directly study the link between folding and catalysis in small ribozymes due to the difficulty of temporally controlling their activity. Reassembly of the ribozyme from separate strands can be inefficient (10), and sequential refolding can initially increase conformational heterogeneity (11).

Photocaged nucleotides circumvent this challenge by temporally controlling RNA function through light-activated removal of a protecting group (12–15). Photoreactive purines have been used to study ligand binding to the purine riboswitch, refolding transition states, and RNA base pairing by an RNA chaperone (16–19). Most photocaged nucleotides contain altered hydrogen bonding patterns from the native molecule that they disguise, but perturbation of π-stacking has also been utilized to control structure and function (20, 21). Variations of the *o*-nitrobenzyl photoredox reaction have proven to be valuable tools for temporally controlling nucleic acid structure and function. However, the half-life for releasing the unmodified nucleotide following the photochemical transformation can be on the seconds timescale, which limits their use in dynamics experiments (13). Photosolvolysis reactions, such as those involving *p*-hydroxyphenacyl protecting groups (e.g., ref. 1 and Fig. 1*A*), release their cargo in less than one microsecond (13) and should be useful for probing processes occurring on the submillisecond timescale. We previously employed a UV-activated variant of **1** to temporally modulate RNA base pairing by the RNA chaperone Hfq (18).

Here, we report a modified *p*-hydroxyphenacyl protecting group for guanosine O6 that is cleaved using 405-nm light (ref. 1 and Fig. 1*A*). This nucleotide provides spatial-temporal control over ribozyme function when used in conjunction with single-molecule observation by total internal reflection fluorescence (TIRF) microscopy. We applied this photocage strategy to the *Oryza sativa* twister ribozyme (25), a 54-nt self-cleaving RNA, which can be easily modified while maintaining its high activity in vitro (22, 26, 27). The small size and fast (~3–10 min^{-1}) self-cleavage of *O. sativa* twister (27–29) make it an ideal model for the correspondence

Significance

Small ribozymes are widespread in nature and have been engineered for artificial gene control in biotechnology and therapeutic applications. To understand how these simple RNA motifs work, we designed and synthesized a chemically protected "photocaged" nucleotide that blocks ribozyme folding until the block is removed with a short (≤0.03 s) pulse with a blue laser. We combined this tool with a microscope capable of observing single RNA molecules and showed that photocaged ribozymes can be turned on with light more precisely and more quickly than was previously possible. This tool for controlling RNA with light allows the ribozyme reaction pathway to be observed in real time and can be applied to other RNA-based systems for gene control.

Author contributions: A.K., H.S., J.N.C., S.P., T.H., M.M.G., and S.A.W. designed research; A.K., H.S., B.H., H.Y., J.N.C., and R.P. performed research; H.S., S.P., and M.M.G. contributed new reagents/analytic tools; A.K. and B.H. analyzed data; and A.K., M.M.G., and S.A.W. wrote the paper.

The authors declare no competing interest.

This article is a PNAS Direct Submission.

[1]A.K. and H.S. contributed equally to this work.

[2]Present address: Process Development Analytics, Bristol-Meyers Squibb, Devens, MA 01434.

[3]Present address: School of Pharmacy, Tianjin Medical University, 300070 Tianjin, People's Republic of China.

[4]Present address: Chemistry Department, Syngene International, Bengalaru 560 099, India.

[5]Present address: Research and Development, GeneDx, Gaithersburg, MD 20877.

[6]To whom correspondence may be addressed. Email: mgreenberg@jhu.edu or swoodson@jhu.edu.

This article contains supporting information online at https://www.pnas.org/lookup/suppl/doi:10.1073/pnas.2003425117/-/DCSupplemental.

First published May 19, 2020.

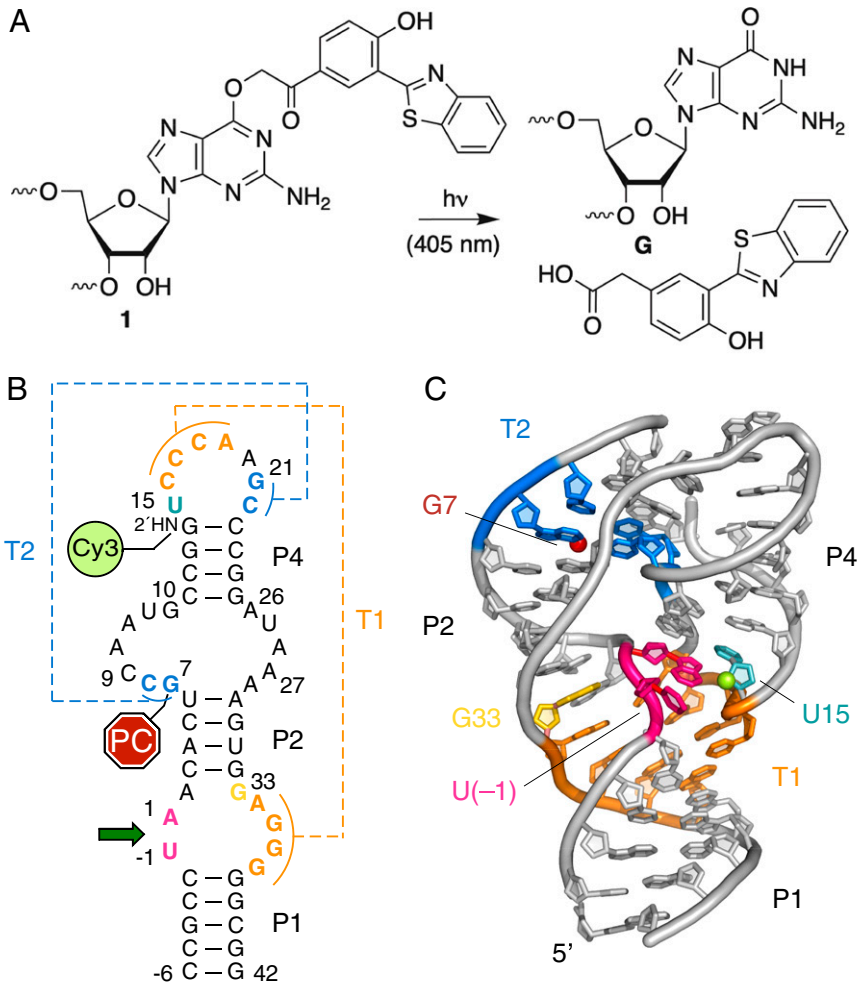

Fig. 1. Photocaged guanosine controls tertiary folding of twister ribozyme. (*A*) Photocaged guanosine **1** is unable to participate in Watson–Crick hydrogen bonding (*Left*). **1** is converted to guanosine upon excitation with 372- to 405-nm light. See *SI Appendix* for synthesis details. (*B*) Secondary structure of *O. sativa* twister ribozyme indicating paired (P) helices and pseudoknots T1 (orange) and T2 (blue), which are necessary for self-cleavage between U(–1) and A1 (pink). G33 (gold) participates in twister self-cleavage. Cy3 is attached to the 2′ position of U15 (teal). The PC is attached to the O6 of G7. The sequence is numbered according to refs. 22, 23. (*C*) Three-dimensional structure colored as in *B* from Protein Data Bank ID code 4OJI (24). Red sphere indicates photocage attachment; green sphere indicates Cy3 attachment point.

between folding and catalysis in RNA. The real-time observation of twister folding and self-cleavage achieved with this photocaging strategy reveals how metal ions tune the energy landscape for ribozyme function.

Results

Synthesis and Validation of a Photocaged Guanosine for Rapid Control of RNA Base Pairing. Photocaged **1** presents a distinct hydrogen bonding pattern from guanosine and is an attractive tool for studying dynamics due to the rapid release of the native nucleotide following photolysis. Longer wavelength absorptivity (≥400 nm) was required to adapt this tool for single-molecule TIRF microscopy experiments, and a recent report indicated that the benzothiazole group would fulfill this requirement (23). The viability of **1** as a photocaged precursor for guanosine was established by photolyzing the nucleoside in aqueous methanol (1:1) using light-emitting diodes (395–405 nm). Reverse-phase HPLC analysis indicated that **1** was quantitatively transformed into guanosine within 5 min of irradiation (*SI Appendix*, Fig. S1). Oligonucleotides containing **1** were prepared via solid-phase synthesis (*SI Appendix*, Fig. S2). Twister ribozymes were then assembled via enzyme ligation of the desired oligonucleotides and purified by denaturing PAGE (*Materials and Methods* and *SI Appendix*, Table S1 and Fig. S3 *A* and *B*).

Photocaged Guanosine Controls Ribozyme Self-Cleavage. The tertiary structure of *O. sativa* twister ribozyme is defined by two conserved pseudoknots, T1 and T2 (Fig. 1 *B* and *C*; orange and blue), which pin the RNA into a compact shape, and which are needed for cleavage between nucleotides U(–1) and A1 (pink) (25, 28, 30). Crystal structures of twister ribozymes were obtained using 2′-deoxyribose at the active site to block self-cleavage, with the result that the crystallized RNA was not in the reactive conformation (24, 28, 30). Chemical mutagenesis experiments and molecular dynamics (MD) simulations, however, suggest a likely structure of the transition state for self-cleavage (29, 31, 32). In addition to formation of the pseudoknots, U(–1) must stack under G33, positioning the N1 of G33 to activate the 2′ O of U(–1) for nucleophilic attack on the adjacent phosphodiester, while the A1 N3 stabilizes the leaving product (29, 33) (Fig. 1*C*).

Since single mutations in pseudoknot T2 block folding (25, 27), we introduced the photocaged (PC) guanosine **1** into *O. sativa* twister at position G7 (G7PC) in the T2 pseudoknot (Fig. 1*C*). G7PC blocked self-cleavage as intended (*SI Appendix*, Fig. S3*C*). After the G7PC RNA was exposed to blue light, we

observed the expected products of twister self-cleavage, indicating that the ribozyme could regain activity after photo-deprotection (*SI Appendix*, Fig. S3*C*).

Light-Controlled Ribozymes with Single-Molecule Detection. We next used TIRF microscopy to study the folding kinetics of single twister ribozymes after photo-deprotection (Fig. 2). Ribozymes were immobilized on a passivated quartz slide via a 5′ biotinylated DNA oligomer complementary to a 38-nt 3′ DNA extension of the twister sequence (*SI Appendix*, Table S1 and ref. 27). To monitor folding, a Cy5 acceptor fluorophore was attached to the 3′ end of the DNA tether and a Cy3 donor fluorophore was attached to the 2′ position of U15, which is adjacent to pseudoknot T1 (Fig. 1*D*). These two positions are ~31 Å apart in the tertiary structure of twister but >60 Å apart in its secondary structure, resulting in a large increase in FRET efficiency upon folding. A similar attachment of fluorophores was used to monitor folding of the *env-22* twister ribozyme (10). TIRF smFRET experiments with *O. sativa* twister RNA lacking a photocage but containing a 2′-deoxyribose at U(–1) to block cleavage ("dU") confirmed that the fluorophore-labeled ribozyme transitions between an unfolded, low FRET conformation and a folded, high FRET conformation (*SI Appendix*, Fig. S4). The attachment of Cy3 to U15 2′ OH did not impede self-cleavage but slightly raised the Mg^{2+} midpoint for activity to 190 ± 10 μM, from 65 μM for the unlabeled ribozyme (*SI Appendix*, Fig. S5).

To control twister folding with light, a 405-nm laser aligned with the TIRF observation area was used to deprotect photocaged dU-G7PC ribozymes tethered to the slide surface (Fig. 2). Before 405-nm irradiation, most of the molecules were in the unfolded, low FRET state (Fig. 2*A*). After a 250-ms exposure to the 405-nm laser, however, a large population of molecules attained the folded, high FRET state, as judged by the appearance of bright spots in the Cy5 channel (Fig. 2*A*). The uncaging reaction was confined to defined fields of view (FOV) with no noticeable increase in high FRET molecules in adjacent areas of the slide, thereby allowing multiple FOVs to be imaged in a single slide channel.

At 2 mM $MgCl_2$, at which 74% of noncaged dU ribozymes are folded (Fig. 2 *B*, *Top*), the photocaged dU G7PC molecules remained unfolded, with virtually none in the high FRET conformation (Fig. 2 *B*, *Middle*). After 0.25 s of 405-nm exposure, the population of folded molecules increased to 56% (Fig. 2 *B*, *Bottom*), corresponding to ~75% activation compared with the noncaged dU ribozyme in the same conditions. Repeated exposure of the same FOV increased the folded population by 10–15% (*SI Appendix*, Fig. S6). In an experiment with photocaged cleavable "rU"–1 ribozymes, the yield of folded ribozyme was nearly saturated by a single 30-ms exposure (*SI Appendix*, Fig. S6). Thus, the photocaged guanosine **1** allows for rapid light activation of RNA folding with spatial precision.

For those molecules that were activated by the 405-nm exposure, the FRET efficiencies of the unfolded and folded populations (Fig. 2*B*) and the folding rate constants (*SI Appendix*, Table S2) were equal to those of the noncaged dU ribozyme. This result plus the recovery of self-cleavage activity suggested that uncaging releases the native ribozyme containing G7.

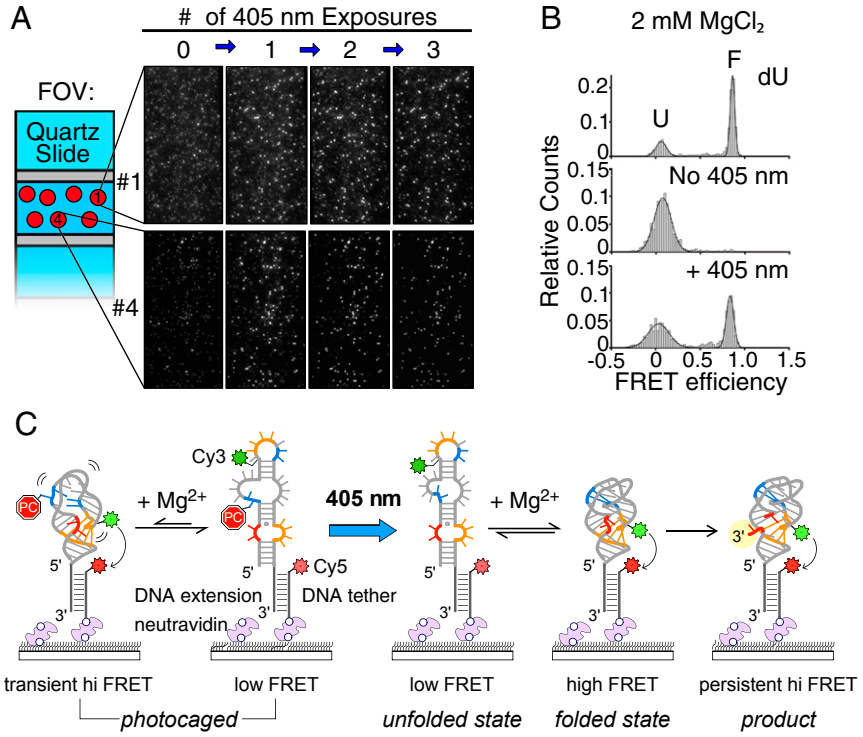

Fig. 2. Spatial and temporal control of single twister ribozymes with light. (*A*) Twister ribozymes containing a photocaged guanosine (G7PC) were immobilized on a quartz slide. Each FOV, ~75 μm × 37 μm, was illuminated by the 405-nm laser (19 mW output) three times (0.25 s each), then imaged in the Cy5 channel with Cy3 excitation. Without 405-nm exposure, there are few bright spots in the Cy5 channel. After a 0.25-s exposure, molecules become bright as they fold into a high FRET state. Upper row, first FOV; lower row, fourth FOV that was exposed to 405 nm in the same experiment. Some molecules are photobleached upon repeated exposure. (*B*) Population of folded ribozyme molecules at 2 mM $MgCl_2$. (*Top*) Noncaged dU ribozyme. (*Middle*) dU-G7PC before exposure. (*Bottom*) Same 2 min after 0.25-s 405-nm exposure. In this experiment, ~56% of molecules are in the high FRET state. Histograms were built from 2,500 to 3,000 molecules selected at random from each FOV (*SI Appendix*). (*C*) Light-controlled folding. The PC (red octagon) obstructs pseudoknot T2 (blue), favoring the low FRET state except for brief visits to high FRET states. After the PC is removed by 405-nm light, twister fluctuates into the high FRET tertiary structure and self-cleaves, forming a persistent high FRET product.

Detecting Folding and Self-Cleavage of Twister Ribozyme. We next used our light-activated system to determine the probability that twister will self-cleave under various folding conditions, by recording the FRET efficiency of cleavable "rU" G7PC ribozymes before and after a 405-nm exposure (Fig. 3*A*). Before the 405-nm flash, we only detected molecules in the low FRET state in 0.1–0.5 mM $MgCl_2$ (Fig. 3 *A* and *B* and *SI Appendix*, Fig. S7). In 100 mM $MgCl_2$, frequent fluctuations into mid to high FRET states suggested that the caged ribozyme transiently forms more compact structures, but these structures are not stable due to the photocaged G (**1**) (*SI Appendix*, Fig. S8). Such partially folded states may be too short-lived at lower Mg^{2+} concentrations to be observed in our TIRF experiment.

Following release of the photocage with the 405-nm flash, the activated ribozymes were able to transition to the high FRET state. As expected, the folded population after uncaging increased with $MgCl_2$ concentration (Fig. 3*E* and *SI Appendix*, Fig. S7). Sometimes the ribozyme unfolded again within a few seconds, whereas other times, the RNA persisted in the high FRET state for the remainder of the movie (Fig. 3*A*). In agreement with studies of *env-22* twister (10), we interpret this persistent high FRET state to represent the cleaved product, because twister ribozymes that were allowed to self-cleave before immobilization also remained in the high FRET state, even after the addition of 50 mM EDTA (*SI Appendix*, Fig. S9). In contrast, we never observed persistent high FRET for the noncleavable dU ribozyme within 0–2 mM $MgCl_2$ range covering the folding transition (Fig. 3 *C* and *D* and *SI Appendix*, Fig. S7*A*). Thus, upon light activation, a twister ribozyme may fold unproductively and quickly unfold, or it may attain the active conformation and form stably folded product.

Rate of Ribozyme Folding and Cleavage under Different $MgCl_2$ Concentrations. Ribozyme efficiency depends on the speed of folding and the likelihood that a folding event will result in self-cleavage. To determine the efficiency of twister ribozyme, we measured the initial folding time and the observed cleavage time at three $MgCl_2$ concentrations spanning the folding equilibrium. The initial folding time was defined as the interval between the 405-nm flash and the first transition into the high FRET state (Fig. 4*A*). The cumulative distribution of folding times was fit to an exponential rate equation to obtain folding rate constants (*SI Appendix*, Fig. S10). Similarly, the rate of productive folding and self-cleavage was defined as the interval from the 405-nm flash until the start of a persistent (≥30 s) high FRET state (Fig. 4*A*). Only molecules that ultimately achieved a persistent high FRET state during the movie were included in this analysis to eliminate RNA molecules that were not uncaged.

For the uncaged molecules, the initial folding rate, k_F, increased as $MgCl_2$ concentration increased, suggesting that divalent ions stabilize the folding transition state or a high energy folding intermediate (Fig. 4 *B* and *C*, black symbols). The increase in k_F with $MgCl_2$ concentration was fit to a linear free energy model, yielding $n_f^{\ddagger} = \partial \Delta k_F / \partial \ln[Mg^{2+}] \sim 0.4$ at 20 °C. For twister molecules that fluctuated several times between the unfolded and folded states before self-cleaving, the rate of the first folding attempt (0.021 ± 0.0003 s^{-1} in 0.1 mM $MgCl_2$) was similar to the average folding rate (0.024 ± 0.0003 s^{-1}) and the

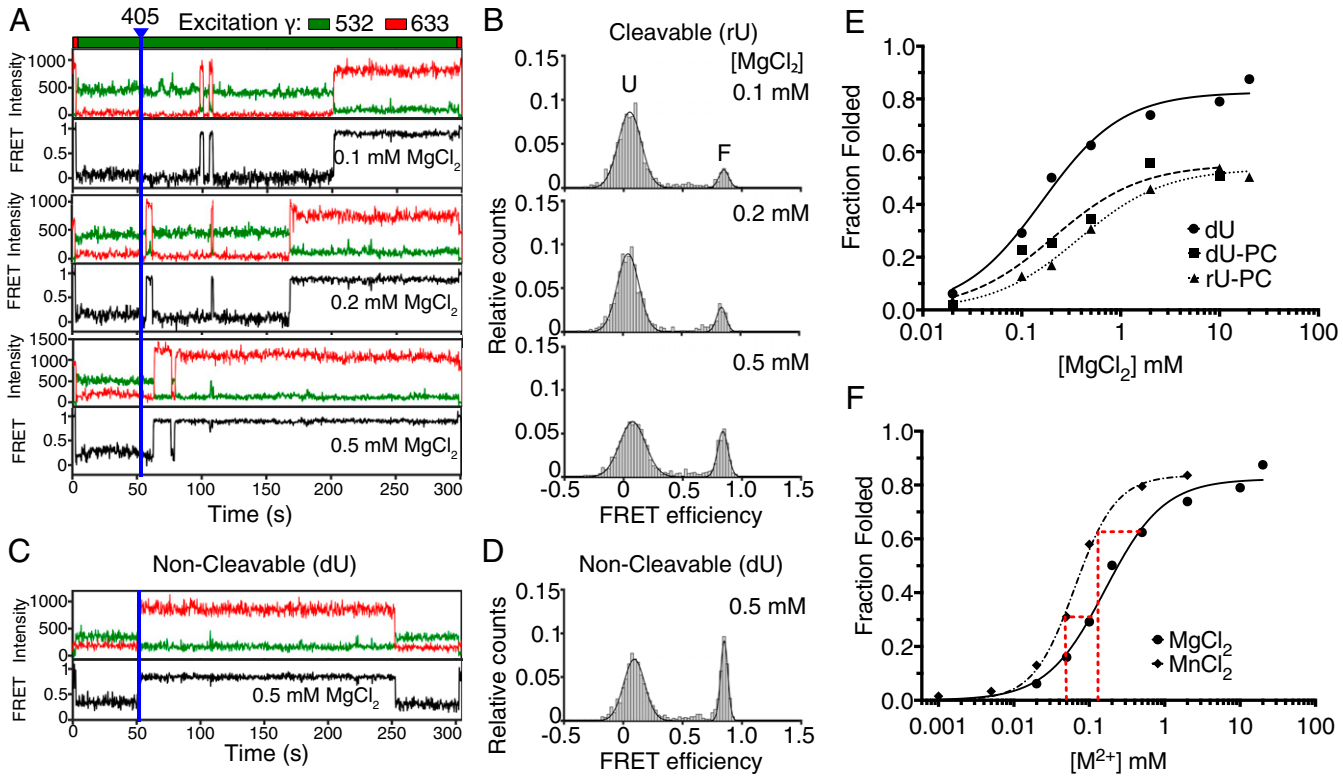

Fig. 3. Light activation of twister ribozyme reveals the coupling between folding and self-cleavage. (*A*) Sample trajectories of rU-G7PC twister under different $MgCl_2$ concentrations. Top bar indicates the laser excitation sequence; blue line represents the time of 0.25-s, 405-nm illumination. Green, Cy3 intensity; red, Cy5 intensity; black, FRET. (*B*) Population histograms of rU twister 2 min after 405-nm exposure in selected $MgCl_2$ concentrations; see *SI Appendix*, Fig. S7 for additional data. (*C* and *D*) Representative data for dU-G7PC twister in 0.5 mM $MgCl_2$ as in *A* and *B*. The dU ribozyme never enters the persistent high FRET state. See *SI Appendix*, Fig. S7 for additional data. (*E*) $MgCl_2$-dependent folding of twister from smFRET. The high FRET population, f_F, was fit to a Hill equation in which $[Mg^{2+}]_{1/2}$ is the midpoint and n is the gradient, $\partial f_N / \partial [Mg^{2+}]$. dU (noncaged): $[Mg^{2+}]_{1/2} = 0.16 \pm 0.024$ mM and $n = 1$; dU-PC (caged): $[Mg^{2+}]_{1/2} = 0.21 \pm 0.083$ mM $MgCl_2$; rU-PC (caged): $[Mg^{2+}]_{1/2} = 0.37 \pm 0.06$ mM $MgCl_2$. The rU high FRET population includes cleaved and uncleaved molecules. (*F*) Folding of noncaged dU ribozyme in $MnCl_2$; $[Mn^{2+}]_{1/2} = 0.064 \pm 0.004$ mM and $n = 1.6 \pm 0.15$. Red lines show isostable conditions.

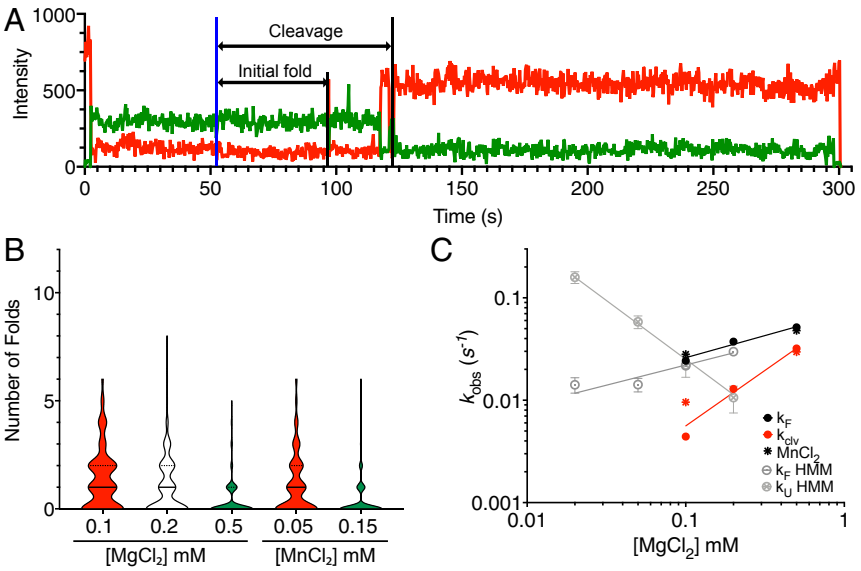

Fig. 4. Folding conditions modulate ribozyme efficiency. (*A*) Sample trace of an rU-G7PC twister molecule, showing the time of photocage activation with a blue line and the initial folding time and cleavage time. The persistent high FRET state at the end of the trace is taken to be the product complex. (*B*) Number of folding events per molecule prior to self-cleavage in various divalent ion concentrations. Solid lines, median; dotted lines; quartiles. Colors indicate isostable conditions. (*C*) Kinetic landscape for ribozyme activity. The observed rate constants were fit to a linear free energy model, in which the activation free energy $\Delta G^{\ddagger} = (\ln k_{ref} + n^{\ddagger}\ln[Mg^{2+}])/k_B T$, k_B is the Boltzmann constant and T is temperature. Black circles, unproductive folding rate, k_F, for rU-PC after uncaging; black star, k_F in 0.05 mM $MnCl_2$; red circles and red star, cleavage rate k_C in $MgCl_2$ and $MnCl_2$, respectively; gray symbols, k_F and k_U for noncaged dU twister from hidden Markov modeling.

folding rate of the noncaged dU ribozyme (0.022 ± 0.002; *SI Appendix*, Table S2 and Fig. S10), indicating that the photocage does not trap twister in an unfavorable secondary structure. Conversely, the lifetime of the folded dU ribozyme increased with $MgCl_2$ (Fig. 4*C*, gray symbols) as expected (10, 27).

Although the ribozyme folds faster at higher $MgCl_2$, the rate of self-cleavage increased even more steeply with $MgCl_2$ concentration ($n_C^{\ddagger} \sim 1.1$; Fig. 4 *B* and *C*, red symbols). As a result, Mg^{2+} ions increase the "success rate" or efficiency of twister ribozyme. In 0.1 mM $MgCl_2$, self-cleavage is about five times slower than folding, and many molecules fold and unfold several times before they ultimately react (Fig. 4*B*). At 0.5 mM $MgCl_2$, the self-cleavage is almost as fast as folding (Fig. 4 *B* and *C*), and the first observable folding transition often leads to product. In 100 mM $MgCl_2$, most ribozymes fold and react within the 250-ms resolution of the experiment (*SI Appendix*, Fig. S8), indicating that any further energy barrier for self-cleavage is small, once the tertiary structure has formed. That tertiary folding and self-cleavage depend differently on Mg^{2+} shows that these processes reflect different conformational states of the ribozyme, consistent with MD simulations showing that the active site of twister must reorganize before cleavage can occur (32, 33).

Effect of $MnCl_2$ on Twister Ribozyme Folding. We next asked whether other metal ions alter ribozyme efficiency. Mg^{2+} is the second most prominent ion in the cell, behind K^+ (34). Transition metal ions such as Mn^{2+}, however, activate *O. sativa* twister ribozyme at lower concentrations than Mg^{2+} ions (27). One reason could be that transition metals stabilize the ribozyme tertiary structure better. We confirmed that Mn^{2+} stabilized the folded state of the dU twister ribozyme more effectively than Mg^{2+}, based on the lower midpoint (0.064 ± 0.004 mM) and steeper gradient ($n = \partial \ln f_F / \partial \ln[Mn^{2+}] = 1.6$) of the folding transition compared to $MgCl_2$ (0.16 ± 0.021 mM; $n = 1$) (Fig. 3*F*).

Next, the effects of $MnCl_2$ on the initial folding rate and cleavage rate were measured under isostable conditions in which the folding equilibrium of the dU twister ribozyme is equal to that in 0.1 mM or 0.5 mM $MgCl_2$ (Fig. 3*F*). The k_F values were similar at each isostable condition (Fig. 4*C*, black symbols and *SI Appendix*, Table S2), indicating that the reversible folding kinetics depends mainly on the relative stability of the tertiary and secondary structure. Self-cleavage (k_C) was twice as fast in 0.05 mM $MnCl_2$ as in 0.1 mM $MgCl_2$; however, the folding kinetics and equilibrium are the same in these conditions (Fig. 4*C* and *SI Appendix*, Fig. S10). Thus, Mn^{2+} ions particularly favor the active conformation, explaining why *O. sativa* twister is active at low concentrations of transition metals.

Discussion

Small self-cleaving ribozymes are simple yet elegant devices for controlling RNA function that are attractive starting points for therapeutic and biotechnology applications (35–37). The folding pathways of cleavable RNAs have been difficult to study, because they frequently react before they can be observed. Moreover, many small ribozymes must rearrange before self-cleavage to position the active site residues for catalysis and after self-cleavage to ensure product stability (e.g., refs. 3, 38–40). As a result, even small perturbations to the active site residues can alter the balance between reactive and unreactive structures.

Photochemistry has been used to temporally control DNAzymes and ligand-induced folding of a riboswitch (17, 41). However, the uncaging process typically required >30 s, which is too slow to enable studying the folding dynamics of efficient ribozymes such as twister. We developed a tool to control twister ribozymes with visible light that reveals the native ribozyme with sufficient yield after a short irradiation to observe tertiary folding and self-cleavage in real time. Extending the activation wavelength of a *p*-hydroxylphenacyl protecting group into the visible spectrum (405 nm) made the photocaged guanosine **1** compatible with standard total internal reflection or confocal fluorescence microscopes, which should allow its use in single-molecule studies of many RNA and DNA systems. Although the time resolution of our experimental setup was limited to 30 ms, other variants of this photocage are removed on the μs timescale (13), suggesting

that we have not reached the time domain limitations of **1** (13). In addition, this technique allows for multiplexed or high-throughput data collection, since many different fields of view can be activated individually in the same channel.

The results from our light-controlled twister ribozyme provide a clearer view of how metal ions tune the efficiency of RNA catalysis. First, our results show that productive and unproductive folding transitions likely lead to different conformational states of the ribozyme although they have similar FRET values. The main evidence for this is that the probability of folding and self-cleaving (k_C) was twice as sensitive to Mg^{2+} concentration ($n_C^{\ddagger} \sim 1$) as the rate of folding transitions (k_F) that fail to yield product (compare red and black symbols; Fig. 4*C*). This difference in Mg^{2+} sensitivity indicates that the RNA must traverse a different transition state to arrive at the active conformation. The unproductive folding rate k_F was the same within error as the folding rate of the dU ribozyme and presumably represents the frequency of fluctuations into compact tertiary structures that cannot self-cleave (compare black and gray symbols; Fig. 4*C*). Our FRET assay does not distinguish between folded ribozymes that are on the path to the active conformation, yet fail to self-cleave from those structures that are off the main folding path. Nevertheless, this distinction between productive and nonproductive folding is consistent with the observation that self-cleavage requires a conformational change within the active site of twister after the two pseudoknots are formed (10, 29).

Second, our results show that Mg^{2+} ions increase ribozyme efficiency by reducing the number of times that individual ribozymes must fold and unfold before they react (Fig. 4*B*). Extrapolation of k_C and k_F to higher Mg^{2+} concentrations in Fig. 4*C* suggests that k_C exceeds k_F above 1 mM $MgCl_2$, consistent with our earlier results (27). Above 0.5 mM Mg^{2+}, many molecules self-cleave the first time they fold. Although Mg^{2+} ions are not specifically required for catalysis (25, 29, 31), they increase twister activity by increasing the likelihood that the active conformation will be achieved in the first place.

Third, our results show that transition metals activate *O. sativa* twister more effectively than Mg^{2+}. This is not simply owing to a difference in the stability of the tertiary structure in Mg^{2+} and Mn^{2+}. Instead, Mn^{2+} reduces the number of unproductive folding attempts by the cleavable ribozyme compared to a Mg^{2+} solution in which the stability of the dU ribozyme is the same (Fig. 4 *B* and *C*). Thus, metal ions can differently tune the landscape for folding and self-cleavage, thereby altering ribozyme efficiency.

Finally, our results unexpectedly revealed that the 2′ OH at the cleavage site raises the cost for tertiary folding prior to self-cleavage. The effect of the ribose is most evident from the shorter lifetime of the folded rU ribozyme precleavage (higher k_U) compared with the lifetime of the folded dU ribozyme under the same conditions. The greater cost of folding and activating the rU ribozyme likely contributes to the higher $[Mg^{2+}]_{1/2}$ overall (0.37 ± 0.056 mM $MgCl_2$ for rU vs. 0.21 ± 0.06 mM for dU), although the high FRET population of the rU ribozyme also includes many cleaved molecules. This difference could be due to greater configurational entropy in the dU ribozyme (42), or a steric clash of the 2′-OH that forces the rU ribozyme into a higher energy conformation.

The short lifetime of the folded rU ribozyme prior to self-cleavage suggests that tertiary interactions within twister elevate the chemical potential of the precleaved state, akin to substrate destabilization in enzymes (43). The cleaved product of twister is unusually stable, preventing religation and unfolding, as observed for the HDV ribozyme (38). Interestingly, both ribozymes encode dual pseudoknots that provide a sturdy framework for distorting the reactive phosphodiester. New chemical tools such as **1** can begin to reveal how certain RNAs form structures capable of rapid self-cleavage.

Materials and Methods

Photocaged RNA Preparation. All RNA sequences were based on the 54-nt *O. sativa* twister ribozyme, 5′-r(CCGCCUAACACUGCCAAUGCCGGUCCCAAGCCCGG AUAAAAGUGGAGGGGGCGG) plus a 38-nt DNA 3′ extension, "SA5," d(AGGAC-GACACACTTTGG ACAGGACACACAGGACACAGG), resulting in a 92-nt-long *Ost* Twister-SA5 RNA. The full-length photocaged ribozyme was prepared by ligation of synthetic oligonucleotides (*SI Appendix*, Fig. S2 and Table S1). All procedures with the photocaged RNA were done in low light to prevent the photocage from being activated.

Twister Activity Assays. All activity assays were done in 1× HK buffer (30 mM K-Hepes, pH 7.5 at 20 °C; 100 mM KCl) as previously described (27), using the extended twister ribozyme with biotin-DNA tether prepared in the same manner as for smFRET (see below and *SI Appendix* for details). Reactions were quenched with 50 mM EDTA and products were resolved by denaturating 10% PAGE.

Single-Molecule FRET. Biotin-SA5-Cy5 was annealed with the 3′ SA5 extension. In a 10-μL reaction, 40 nM twister RNA was combined with 20 nM biotin-SA5-Cy3 DNA in 1× HK Buffer with 12 U RNasin Plus. The reaction was incubated at 75 °C for 5 min, 37 °C for 15 min, 25 °C for 5 min, and then kept at room temperature. The mixture was diluted 700-fold in 1× HK buffer and loaded right away onto a covered quartz slide passivated with dichlorodimethylsilane (Sigma, catalog no. 440272), 0.2 mg/mL biotin-BSA (Sigma catalog no. A8549-10MG), 2% Tween 20, and 0.2 mg/mL streptavidin (44). After 1 min, unbound RNA was washed away with imaging buffer containing 1× HK, $MgCl_2$, or $MnCl_2$, plus 0.8% glucose, 4 mM Trolox, 0.1 mg/mL glucose oxidase, and 0.02 mg/mL catalase to minimize photobleaching. The data were acquired using a home built prism-TIRF microscope (42) with a 405-nm, 532-nm, and 633-nm laser (*SI Appendix*).

Single-Molecule Data Analysis. Molecules with active Cy3 and Cy5 fluorophores were selected for analysis, and FRET efficiency was calculated after corrections for background, reflection, leakage, and direct excitation. The folded population was obtained from Gaussian fits to histograms of FRET efficiency as previously described in ref. 45. The times of initial folding and cleavage after the 405-nm exposure were analyzed by hand within MatLab (*SI Appendix*). The frequency distributions of the dwell times for folding and cleavage events were fit to an exponential decay to obtain rate constants for initial folding, self-cleavage, and folding at different $MgCl_2$ concentrations.

Data Availability. Analyzed data and primary data are available upon request to the corresponding authors.

ACKNOWLEDGMENTS. We thank M. Rodgers and I. M. Sharma for their assistance, and members of the S.A.W. laboratory for helpful discussion. This work was supported by NSF Grants MCB-1616081 (to M.M.G. and S.A.W.) and PHY-1430124 (to T.H.); and National Institute of General Medicine Grants R01 GM-063028, R01 GM-054496 (to M.M.G.), and R35 GM-122569 (to T.H.). T.H. is an Investigator with the Howard Hughes Medical Institute.

1. R. M. Jimenez, J. A. Polanco, A. Lupták, Chemistry and biology of self-cleaving ribozymes. *Trends Biochem. Sci.* **40**, 648–661 (2015).
2. E. Tan *et al.*, A four-way junction accelerates hairpin ribozyme folding via a discrete intermediate. *Proc. Natl. Acad. Sci. U.S.A.* **100**, 9308–9313 (2003).
3. M. K. Nahas *et al.*, Observation of internal cleavage and ligation reactions of a ribozyme. *Nat. Struct. Mol. Biol.* **11**, 1107–1113 (2004).
4. M. J. Fedor, Tertiary structure stabilization promotes hairpin ribozyme ligation. *Biochemistry* **38**, 11040–11050 (1999).
5. A. A. Andersen, R. A. Collins, Rearrangement of a stable RNA secondary structure during VS ribozyme catalysis. *Mol. Cell* **5**, 469–478 (2000).
6. M. De la Peña, S. Gago, R. Flores, Peripheral regions of natural hammerhead ribozymes greatly increase their self-cleavage activity. *EMBO J.* **22**, 5561–5570 (2003).
7. A. Khvorova, A. Lescoute, E. Westhof, S. D. Jayasena, Sequence elements outside the hammerhead ribozyme catalytic core enable intracellular activity. *Nat. Struct. Biol.* **10**, 708–712 (2003).
8. G. Pljevaljcić, D. Klostermeier, D. P. Millar, The tertiary structure of the hairpin ribozyme is formed through a slow conformational search. *Biochemistry* **44**, 4870–4876 (2005).
9. N. Girard, P. Dagenais, J. Lacroix-Labonté, P. Legault, A multi-axial RNA joint with a large range of motion promotes sampling of an active ribozyme conformation. *Nucleic Acids Res.* **47**, 3739–3751 (2019).

10. N. Vušurović, R. B. Altman, D. S. Terry, R. Micura, S. C. Blanchard, Pseudoknot formation seeds the twister ribozyme cleavage reaction coordinate. *J. Am. Chem. Soc.* **139**, 8186–8193 (2017).
11. B. Hua, S. Panja, Y. Wang, S. A. Woodson, T. Ha, Mimicking co-transcriptional RNA folding using a superhelicase. *J. Am. Chem. Soc.* **140**, 10067–10070 (2018).
12. C. Brieke, F. Rohrbach, A. Gottschalk, G. Mayer, A. Heckel, Light-controlled tools. *Angew. Chem. Int. Ed. Engl.* **51**, 8446–8476 (2012).
13. P. Klán *et al*., Photoremovable protecting groups in chemistry and biology: Reaction mechanisms and efficacy. *Chem. Rev.* **113**, 119–191 (2013).
14. A. Rodrigues-Correia, D. Knapp-Bühle, J. W. Engels, A. Heckel, Selective uncaging of DNA through reaction rate selectivity. *Org. Lett.* **16**, 5128–5131 (2014).
15. P. Seyfried *et al*., Optimal destabilization of dna double strands by single-nucleobase caging. *Chemistry* **24**, 17568–17576 (2018).
16. P. Wenter, B. Fürtig, A. Hainard, H. Schwalbe, S. Pitsch, Kinetics of photoinduced RNA refolding by real-time NMR spectroscopy. *Angew. Chem. Int. Ed. Engl.* **44**, 2600–2603 (2005).
17. J. Buck, B. Fürtig, J. Noeske, J. Wöhnert, H. Schwalbe, Time-resolved NMR methods resolving ligand-induced RNA folding at atomic resolution. *Proc. Natl. Acad. Sci. U.S.A.* **104**, 15699–15704 (2007).
18. S. Panja, R. Paul, M. M. Greenberg, S. A. Woodson, Light-triggered RNA annealing by an RNA chaperone. *Angew. Chem. Int. Ed. Engl.* **54**, 7281–7284 (2015).
19. B. Fürtig *et al*., Refolding through a linear transition state enables fast temperature adaptation of a translational riboswitch. *Biochemistry* **59**, 1081–1086 (2020).
20. M. J. E. Resendiz, A. Schön, E. Freire, M. M. Greenberg, Photochemical control of RNA structure by disrupting π-stacking. *J. Am. Chem. Soc.* **134**, 12478–12481 (2012).
21. J. M. N. San Pedro, M. M. Greenberg, Photochemical control of DNA structure through radical disproportionation. *ChemBioChem* **14**, 1590–1596 (2013).
22. J. Gebetsberger, R. Micura, Unwinding the twister ribozyme: From structure to mechanism. *Wiley Interdiscip. Rev. RNA* **8**, e1402 (2017).
23. S. Barman *et al*., A p-Hydroxyphenacyl–benzothiazole–chlorambucil conjugate as a real-time-monitoring drug-delivery system assisted by excited-state intramolecular proton transfer. *Angew. Chem. Int. Ed. Engl.* **55**, 4194–4198 (2016).
24. D. Eiler, J. Wang, T. A. Steitz, Structural basis for the fast self-cleavage reaction catalyzed by the twister ribozyme. *Proc. Natl. Acad. Sci. U.S.A.* **111**, 13028–13033 (2014).
25. A. Roth *et al*., A widespread self-cleaving ribozyme class is revealed by bioinformatics. *Nat. Chem. Biol.* **10**, 56–60 (2014).
26. D. M. J. Lilley, How RNA acts as a nuclease: Some mechanistic comparisons in the nucleolytic ribozymes. *Biochem. Soc. Trans.* **45**, 683–691 (2017).
27. S. Panja, B. Hua, D. Zegarra, T. Ha, S. A. Woodson, Metals induce transient folding and activation of the twister ribozyme. *Nat. Chem. Biol.* **13**, 1109–1114 (2017).
28. A. Ren *et al*., In-line alignment and Mg^{2+} coordination at the cleavage site of the env22 twister ribozyme. *Nat. Commun.* **5**, 5534 (2014).
29. T. J. Wilson, Y. Liu, C. Domnick, S. Kath-Schorr, D. M. Lilley, The novel chemical mechanism of the twister ribozyme. *J. Am. Chem. Soc.* **138**, 6151–6162 (2016).
30. Y. Liu, T. J. Wilson, S. A. McPhee, D. M. Lilley, Crystal structure and mechanistic investigation of the twister ribozyme. *Nat. Chem. Biol.* **10**, 739–744 (2014).
31. M. Košutić *et al*., A mini-twister variant and impact of residues/cations on the phosphodiester cleavage of this ribozyme class. *Angew. Chem. Int. Ed. Engl.* **54**, 15128–15133 (2015).
32. C. S. Gaines, D. M. York, Ribozyme catalysis with a twist: Active state of the twister ribozyme in solution predicted from molecular simulation. *J. Am. Chem. Soc.* **138**, 3058–3065 (2016).
33. C. S. Gaines, T. J. Giese, D. M. York, Cleaning up mechanistic debris generated by twister ribozymes using computational RNA enzymology. *ACS Catal.* **9**, 5803–5815 (2019).
34. D. E. Draper, D. Grilley, A. M. Soto, Ions and RNA folding. *Annu. Rev. Biophys. Biomol. Struct.* **34**, 221–243 (2005).
35. M. C. Maurel, F. Leclerc, J. Vergne, G. Zaccai, RNA back and forth: Looking through ribozyme and viroid motifs. *Viruses* **11**, 283 (2019).
36. S. V. Park *et al*., Catalytic RNA, ribozyme, and its applications in synthetic biology. *Biotechnol. Adv.* **37**, 107452 (2019).
37. C. E. Weinberg, Z. Weinberg, C. Hammann, Novel ribozymes: Discovery, catalytic mechanisms, and the quest to understand biological function. *Nucleic Acids Res.* **47**, 9480–9494 (2019).
38. A. Ke, K. Zhou, F. Ding, J. H. Cate, J. A. Doudna, A conformational switch controls hepatitis delta virus ribozyme catalysis. *Nature* **429**, 201–205 (2004).
39. P. B. Rupert, A. R. Ferré-D'Amaré, Crystal structure of a hairpin ribozyme-inhibitor complex with implications for catalysis. *Nature* **410**, 780–786 (2001).
40. C. S. Gaines, J. A. Piccirilli, D. M. York, The L-platform/L-scaffold framework: A blueprint for RNA-cleaving nucleic acid enzyme design. *RNA*, 111–125 (2019).
41. Q. Liu, A. Deiters, Optochemical control of deoxyoligonucleotide function via a nucleobase-caging approach. *Acc. Chem. Res.* **47**, 45–55 (2014).
42. E. J. Denning, A. D. MacKerell Jr, Intrinsic contribution of the 2′-hydroxyl to RNA conformational heterogeneity. *J. Am. Chem. Soc.* **134**, 2800–2806 (2012).
43. D. C. Phillips, The three-dimensional structure of an enzyme molecule. *Sci. Am.* **215**, 78–90 (1966).
44. B. Hua *et al*., An improved surface passivation method for single-molecule studies. *Nat. Methods* **11**, 1233–1236 (2014).
45. R. Roy, S. Hohng, T. Ha, A practical guide to single-molecule FRET. *Nat. Methods* **5**, 507–516 (2008).